ASIA TURBOMACHINERY & PUMP SYMPOSIUM
12 - 15 MARCH 2018
SUNTEC SINGAPORE

ROTORDYNAMICS, DESIGN ASPECTS, FIELD AND OPERATIONAL EXPERIENCES OF A NOVEL, LARGE COMPRESSOR STRING SUPPORTED BY ACTIVE MAGNETIC BEARINGS

Dr. Rainer Gausmann
is Head of a Mechatronics Team within the Siemens Power & Gas Division, Compressor Product Development, in Duisburg, Germany.

His main scope of activity is the design and the rotor dynamics of compressors levitated by active magnetic bearings. During his more than 10 years with this company he has been involved in the design, testing and commissioning of a high-pressure seal test rig, various motor-driven compressors, and the hermetically sealed STC-ECO motorcompressor.
Dr. Gausmann received his Diploma degree in 1997 from the University of Hannover and his doctorate from the Technical University of Karlsruhe in 2005.

Frank Heidtmann
is a Development Engineer within the Siemens Power & Gas Division, Compressor Product Development, in Duisburg, Germany.

After several years as a research associate at the University Duisburg-Essen in the area of control and diagnosis of elastomechanical systems, he joined Siemens in 2009.Since then his activities comprise the full range of rotordynamic-related development work starting from rotor design, simulation and controller synthesis for closed loop controlled compressor plants and continuing with shop as well as field testing and commissioning of such systems. Frank Heidtmann received his Diploma degree in 2003 from the University of Duisburg-Essen.

ABSTRACT

The giant Groningen onshore gas field in the Northeastern Netherlands started production in 1963. About 35 years later, the decreasing reservoir pressure required a first stage of compression to provide sufficient capacity at the required 65 bar (940 psi) grid pressure. Now, a first pilot plant for a second stage of compression is installed in the accelerated cluster Schaapbulten (SCB) and started production end of 2013.

The novel compression string installed consists of a 23-MW synchronous, high-speed motor in a double-end-drive configuration, driving two gearless driven 7- and 8-stage compressors. The approximate 16m (52ft) long train, with about 14mm (0,55inch) axial thermal elongation, is supported by six radial active magnetic bearings (AMBs) and two axial AMBs at the train's non-driven ends.

This contribution deals with the axial, radial and torsional rotordynamics of the AMB-supported string focusing on the two compressors, as well as with string design aspects and latest field / operational experiences. The design aspects touch points like the trade-off in the coupling selection process and resonance frequency optimizations. Field experiences concerning experimental torsional string analysis and run-out effects in combination with the closed loop AMB controller design are presented. Derived and presented improvements have led to an in-detail optimized compressor design and control.

INTRODUCTION

The compressors installed in the depleting Groningen gas field are soon coming to an operational limit in terms of pressure difference between the pipeline pressure and the wellhead pressure. Consequently, an additional compressor was added to the installation.

The existing compression string comprises a 23-MW (30,000hp) synchronous motor and a directly driven inline compressor, both levitated by magnetic bearings. Details are given in Kuemmle et al. (2000). Constraints for the revamp project are the reuse of the existing motor stator and housing and the motor's whole electrical drive and control technology (power supply, switchgears, variable speed drive system, etc.) as well as the existing compressor casing.

In the course of the revamp, a new magnetic bearing system (cf. Walter, et al. (2010)) is introduced into the whole string, comprising a modified double-end-drive motor rotor and a directly driven low-pressure compressor (1st section) on one side and a directly driven high-pressure compressor (2nd section) on the other side of the motor (see Figure 1 and Figure 2). The motor was formerly levitated by three magnetic bearings (two for the main motor and a third one at the exciters non-driven end). The double-end-drive concept asks for a new designed drive through exciter. The third bearing is omitted in the new design, such that the new motor is levitated by only two AMBs.

The control cabinet consists of fully standardized high power inverter technology which is normally used to drive torque motors and linear motors, e.g. in machine tool applications. For the control of a magnetic bearing stator by such a standardized inverter, only the inverter software needed to be modified (cf. Walter, et al. (2010)).

FUNDAMENTALS

The general business trend to operate at higher circumferential speeds in the turbomachinery industry is limited by material properties like the yield strength. Other limitations include

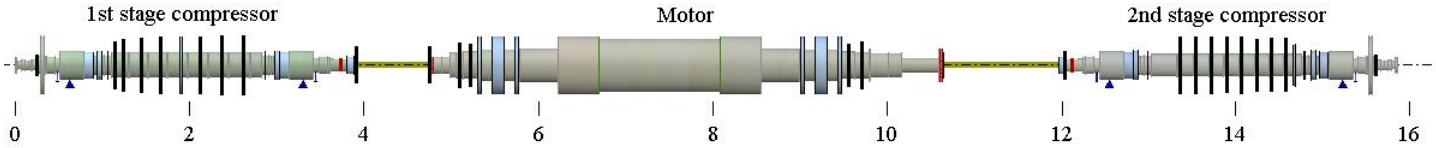

Figure 1. Rotordynamic Model of the 16m Compression String with Directly Attached High Speed Motor, Supported by AMBs

Figure 2. 23-MW (30,000hp) Direct Driven Compression String with Synchronous Motor in Double-End-Drive Configuration, Schaapbulten, Netherlands

excessive pad temperatures and large shear power losses in conventional fluid film bearings. Rotors supported on AMBs have the potential to overcome the last mentioned limitation. Table 1 illustrates a general comparison between fluid film bearings and AMBs.

In contrast to passive fluid film bearings, an AMB is an active component that requires a closed control loop to stabilize the rotor in the center of the air gap between rotor laminations and the AMBs' stator. While the rotordynamic analyses of fluid film bearings is state-of-the-art but afflicted with significant uncertainty in the prediction of dynamic force coefficients for

Table 1. Properties of Oil Lubricated Bearings vs. AMBs

Motor or Turbomachine with	Oil lubricated bearings	Active Magnetic Bearings
Specific load	high	low
Stiffness	high	low
Damping	moderate	high
Circumferential Speed	<100m/s (<330ft/s)	<200m/s (<660ft/s)
Losses	moderate	very low
Speed Range	typically limited	continuous
Complexity	low	high
Environment	Risk to leak	yes
Maintanance	periodical oil and filter checks	nearly no

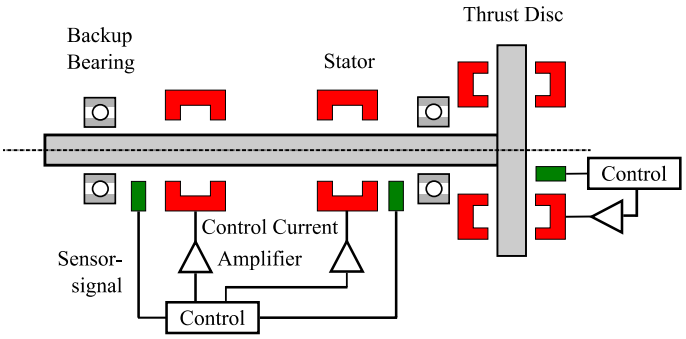

Figure 3: Schematic Representation of a Rotor Supported on AMBs and their Control Loops

tilting pad bearings and gas labyrinth seals (Kocur et al. (2007)), an AMB is highly predictable in terms of its frequency-dependent behavior expressed in the form of a transfer-function (see also later Figure 15), relating the bearing force to the rotor position. This includes the transfer behavior of the sensor (see Figure 3), the amplifier and the force-control current relationship, and the control law, designed individually for each rotor.

QUALIFICATION CAMPAIGN

The magnetic bearing system was successfully full-scale tested in a 5-MW (6,700hp) high-speed asynchronous motor, but in addition needed to be qualified for compressor applications. Together with the end user, a decision was made to perform a qualification based on a Technology Readiness Level (TRL) assessment. Introduced by NASA for space technology, the TRL method has been specifically adapted for different technology fields, for example by API 17N for the oil & gas industry. The TRL process, as used within Shell, is divided into eight levels, including a procedure to assess the maturity of new technologies to avoid and to manage risks in a systematic way. The first four TRL levels, from an unproven concept up to laboratory component development, were considered completed because a spindle and an asynchronous motor were already equipped and running with the newly-developed AMB system. TRL5 is defined as a full-scale component test in a relevant environment and with full interface and functionality tests for the compressor bearings and motor bearings.

The next step (TRL6) is the applied technology qualification (engineering, manufacturing and testing of machinery for

Figure 4. AMBs-Supported Test Compressor

the 23-MW train for an accelerated cluster, a pilot gas processing plant), achieved by fulfilling the requirements of the project's quality control plans. This also includes mechanical running tests as well as Type 1 and Type 2 performance tests of both compressors in the factory, and a factory acceptance test for the driver. TRL7 handles the string design qualification (including installation and commissioning) for the pilot installation. This is achieved by a design review of the integrated string and a third party check of the lateral, axial and torsional dynamics. The next level is TRL8. Therefore, the compression train has to prove reliability and high availability on location during a specific operation period, accompanied by specified tests and activities like robustness tests, power dip tests, 72h full load test, operation map verification, and others.

The compression train successfully passed TRL1 to TRL8, whereby for TRL5 a dedicated full-scale test rig was set up (see Figure 4). The test rig consists of a five-stage compressor (Rating: 23-MW (30,000hp), 120bar (1,741psi) discharge pressure), operating in closed-loop condition with nitrogen and driven by a shop motor with a step-up gear and a mechanical brake (for safety reasons). A comprehensive test program was conducted and successfully passed:

- Axial and radial static load tests
- Axial dynamic load tests
- Unbalance tests
- Gas load test
- Stability tests
- Endurance test
- Radial and axial backup bearing tests
- Advanced safety functions tests

A selection of the tests is roughly presented in the following.

For some tests, special equipment like the axial shear pin tool, shown in Figure 5 and Figure 6, for axial dynamic and

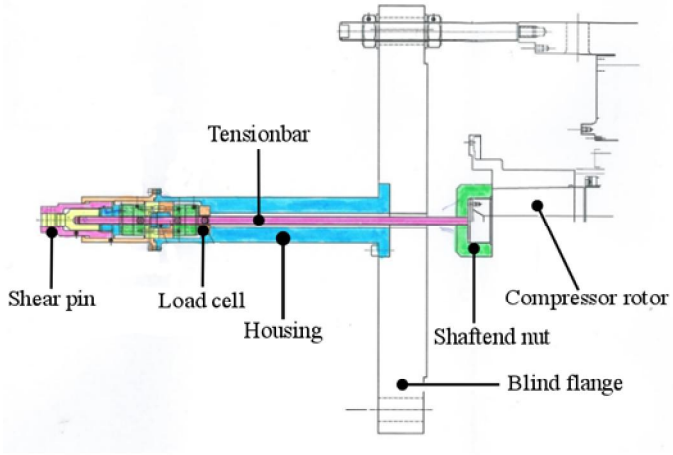

Figure 5. Shear Pin Tool for Static and Dynamic Axial Load Tests

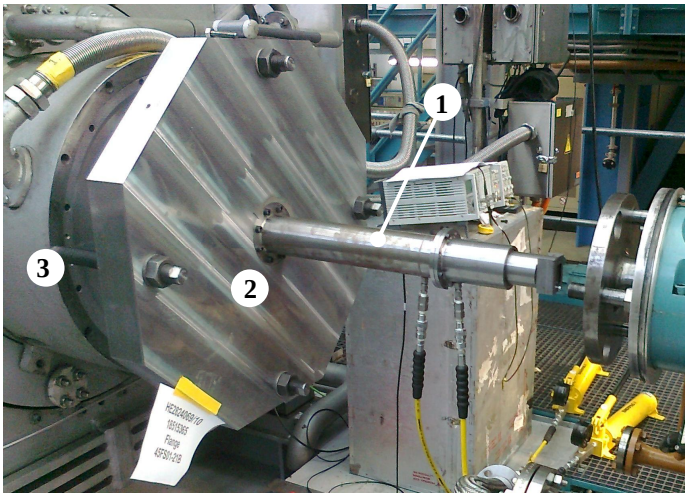

Figure 6. Test Set-Up for Axial Dynamic Step Response Test With Special Tool (1) For Step-Load Application Installed by a Counter Holder (2) at the Compressor Drive-End (3)

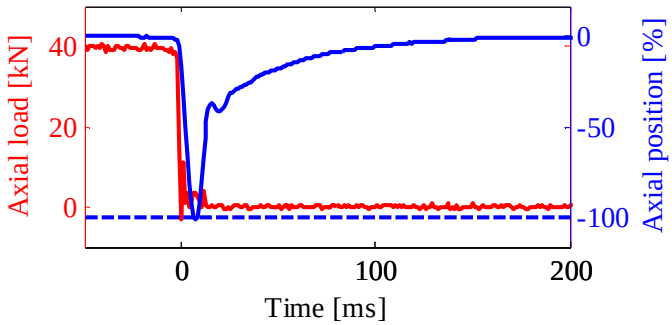

Figure 7. Axial Dynamic Step Response Test by means of 40kN (9,000 lbf) Load-Step; Axial Rotor Position in terms of Backup Bearing Clearance

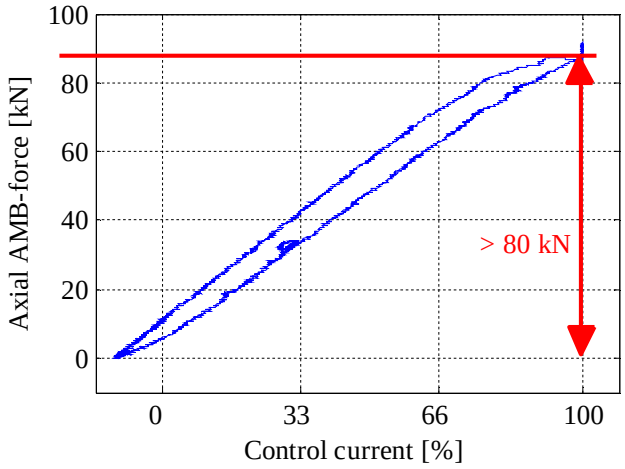

Figure 8. An Axial Static-Load Test Validates more than 80 kN (18,000 lbf) Design Load Capacity

static load tests is designed. This special tool generates an axial load step by means of a shear pin, which breaks at a specific axial test load and thereby rapidly releases a hydraulically generated counterforce, acting against the axial AMB. The load step is measured by a load cell. The corresponding experimental results represent the interaction of the axial AMB, its controller design, and the compressor rotor.

This is of special interest with respect to process upset conditions like surge conditions or any kind of process condition change, e.g. shutting on or off a gas well, change from forward flow to recycle flow, etc. While a stiff behavior of the AMB is generally preferable, its dynamic is constrained by eddy current losses in the solid thrust disc (while the stators are fully laminated for minimized eddy current losses, the thrust disc is solid due to the high circumferential forces). Small and large signal characteristics were investigated, proving linear system behavior and a load-step capability of 40kN (9,000 lbf) before touching the axial backup bearing (see Figure 7). The static axial load test results illustrated in Figure 8 show an excess of the static design force of 80kN (18,000lbf), corresponding to a specific load of about 3.5 bar (50 psi).

The static radial load test is intended to demonstrate the load capacity and was performed by means of a pulling crane force. The test set-up is shown in Figure 9: a rope is wound around the shaft end and connected to a crane with a load cell and a spring. The spring is used to realize a soft connection to the shaft to keep the radial control loop stable and to transform large movements of the crane into small force changes to smoothly adjust the crane force. The crane pulls the spring along the vertical direction while the magnetic bearing system reacts with a counteracting force. The force is measured with a load cell. By taking lever rules, rotor flexibility and the non-collocation of AMB sensors and actuators into account, the forces of the active bearings can be determined from the load cell measurements, Figure 10 shows the result for the x-DE.

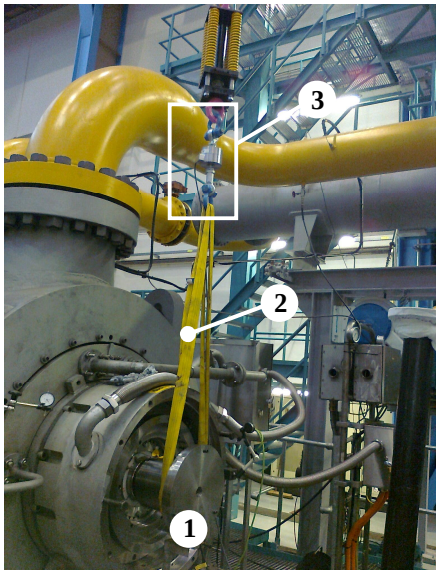

Figure 9. Test Set-Up for Static Radial Load Test at the Uncoupled DE (1) using a Rope (2) and a Load Cell (3) Attached to a Crane for Vertical Pulling

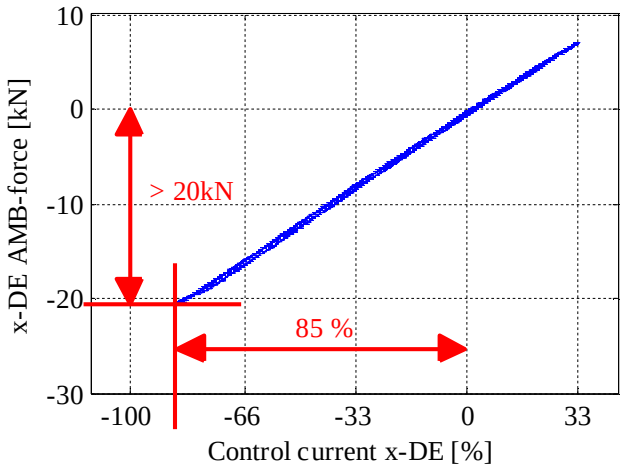

Figure 10. A Radial Static Load Test shows about -20 kN (4,500 lbf) load per Magnetic Axis at 85 Percent Control Current.

About 20kN (4,500 lbf) per magnetic axis at 85 percent of maximum control current was determined (see Figure 10). Due to test set-up restrictions, a full-force test was not possible. A linear extrapolation of the test result indicates a maximum possible magnetic force of about 24kN/axis (5,400 lbf/axis) for the chosen bearing size. This provides a safety factor of about 2.5 with respect to the rotor mass of the 2nd-stage compressor and even more for the 1st-stage compressor.

Also, tests on the backup bearings were performed. The test setup, Figure 4, contains a mechanical brake for safety reasons. This brake is used for a worst case unbalance test: the

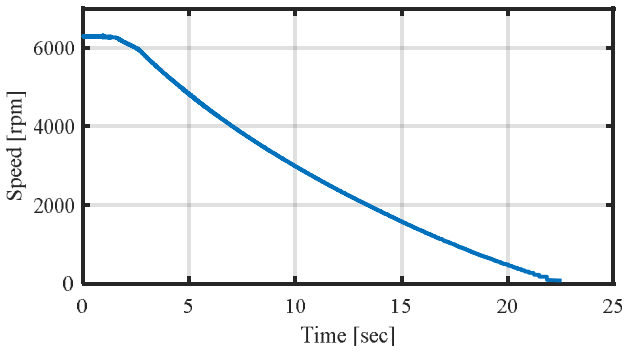

Figure 11. Braked Rundown in Backup Bearings

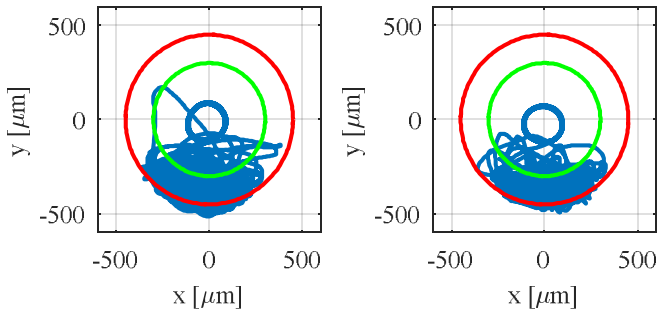

Figure 12. Drive-End (left) and Non-Drive End (right) Orbit Plot of the Braked Shaft Rundown in Backup Bearings with High Unbalance.

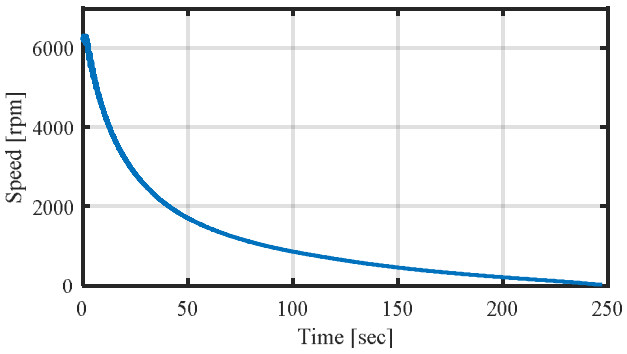

Figure 13. Unbraked Rundown in Backup Bearings

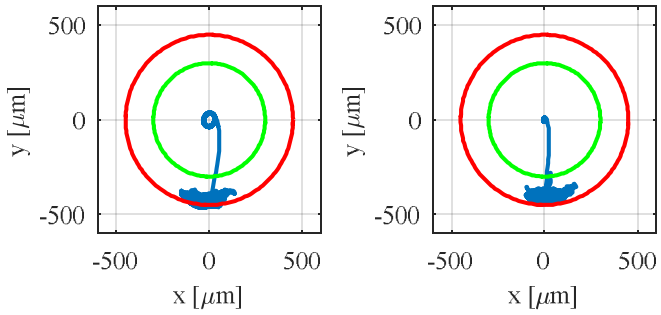

Figure 14. DE (left) and NDE (right) Orbit Plot of the Unbraked Rundown in Backup Bearings with Nominal Unbalance

compressor is running with a worst case unbalance with vibrations close to trip level. In the event of a power loss, the active magnetic bearing system is connected to an uninterruptable power supply (UPS) to ensure a levitated rundown of the compression string. But a total power loss in combination with a malfunction of the UPS is simulated by switching off the magnetic bearing axes at maximum continuous speed. The brake is activated and decelerates the compressor within about 23 sec. to zero speed, see Figure 11. In Figure 12 the shaft vibrations during rundown are shown. Due to the high unbalance, the rotor movement in the lower half of the backup bearings is less confined than in the nominal unbalance case. The green circle shows the nominal clearance of the backup bearing and the red circle the clearance in case the damping feature behind the backup bearing is in a blocked condition.

A final test is conducted to simulate a further failure scenario when the braking system doesn't work. Normally the motor can brake the compression string by regenerative braking. In case of a total power loss and a loss of the UPS, the rotor falls into the backup bearings and performs a free rundown, see Figure 13. The result of this test in terms of an orbit plot is shown in Figure 14. The time to standstill is about 250 seconds. After the test, a condition monitoring run is performed and the backup bearings are assessed to be in a good condition for further use.

FIELD AND OPERATIONAL EXPERIENCES

Radial Sensor Target Material Optimization

The AMB system uses standard eddy current sensors for measuring radial and axial shaft displacements. The pros of this specific choice are industry standard sensors in series quality with high reliability, high and global availability, easily and rapidly replaceable, compact sensor housing and small sensor target surfaces, robust against dust, moisture, pressure and oil.

On the other hand, eddy current measurements are sensitive to sensor target run-out and it is not possible to distinguish real shaft displacements from run-out effects. In consequence, a close loop AMB control reacts on run-out signals as if they were a real shaft displacement. This can result in increased shaft vibrations when the AMB controller reacts on 1x and super-harmonic run-out signals. For an electric coil with inductivity L, (control) current i(t), and (control) voltage u(t), the base equation $u(t) = L\, di(t)/dt$ leads to super-harmonic run-out signals consuming an inverter voltage (inverter modulations depth) linearly increasing with rotor speed. And the more super-harmonic run-out signals are to be processed by the AMB control loop, the more the inverter voltage demand increases, until it is saturated.

Another influence factor on the inverter voltage demand is the AMB controller design. The (single-input, single-output) radial AMB controller transfer functions for the DE and NDE

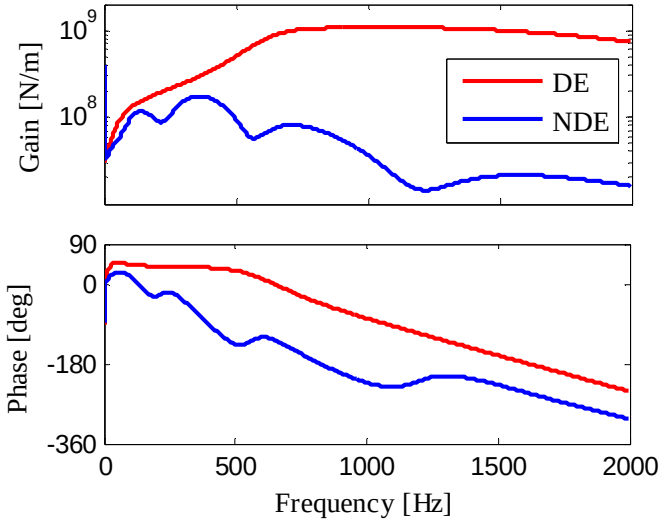

Figure 15. Radial AMB Controller Transfer Function Expressed in Amplitude Response and Phase Response

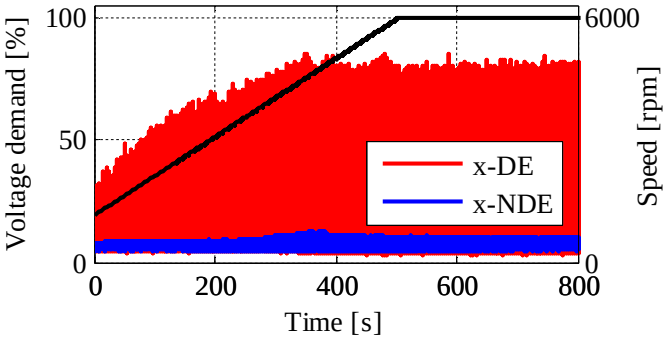

Figure 16. Voltage Demand of AMB Inverters up to 6,000 rpm (100 Percent), x-DE in Comparison to x-NDE Axis

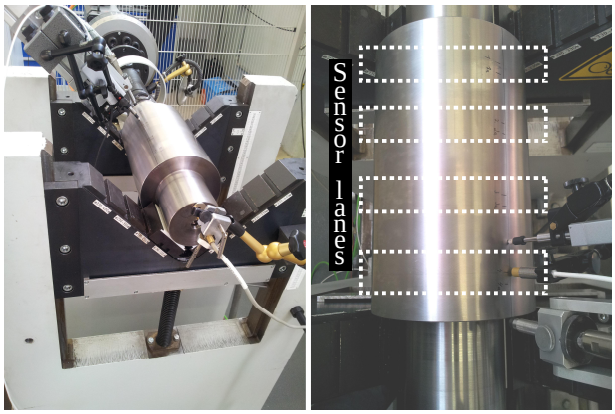

Figure 17. Test-Shaft in a Run-Out Bench (left), and with Four Marked Sensor Target Test-Surfaces (right)

magnetic axes are presented in Figure 15: A narrow-banded controller design with a roll-off close to the second bending mode at NDE has been combined with a broad-banded DE controller design in order to fulfill controller design criteria with respect to AMB stiffness, damping and closed loop robustness. But the controller at DE also amplifies super-harmonic run-out signals in a broad frequency range. And in combination with the given run-out of the sensor target, this turns out to cause an inverter voltage demand of about 80 percent at 6000 rpm (100 percent speed), as shown in Figure 16. In comparison, the narrow-banded NDE controller in combination with similar radial sensor target run-out on NDE leads just to a level of about 10 percent voltage demand.

As the rotordynamic does not allow for a narrow-banded controller design for both DE and NDE, the run-out on DE has to be reduced to increase the inverter saturation margin. A detailed analysis of the sensor target run-out shows that high frequency electrical run-out, caused by inhomogeneous electrical material properties, must be accounted on the relatively high voltage demand on DE. The typical sensor target surface burnishing, used to homogenize the electrical properties of the sensor target surface, did not improve the situation satisfactorily. Therefore, an investigation was started comprising an experimental test series in order to optimize material and manufacturing of the AMB sensor target surfaces. Aspects of this optimization are

- required sensor target depth and width due to material mixing of sensor target and shaft material, eddy current radius of action,
- effects of post treatment by burnishing,
- availability of target material,
- quality, reliability, repeatability, effort, and automation capabilities of the manufacturing process,
- electrical run-out characteristics taking super-harmonics into account,
- measuring sensitivity in combination with the used type of eddy current sensors, further,
- sensor target surfaces shall be embedded (instead of sleeve design) into the base shaft material allowing for thermodynamic advantageous smaller shaft diameters.

Altogether 21 different combinations of material and manufacturing process characteristics were tested by means of six small test-shafts of about 470mm (18.8 inch) length with four sensor test target surfaces each. One of these test-shafts is shown in Figure 17. The test-shaft lies in a run-out bench, is supported by V-blocks with Teflon pads and coupled to an electric drive. The run-out bench is equipped with rotary type encoder, eddy current sensor, and (mechanical) length gauge in order to measure run-out characteristics. On the right hand side of the figure, the four embedded sensor target surfaces of a test-shaft are marked by dotted rectangles.

By measuring the total run-out by means of an eddy current sensor and its mechanical portion by means of an (mechanical) length gauge, the electrical run-out portion can simply be

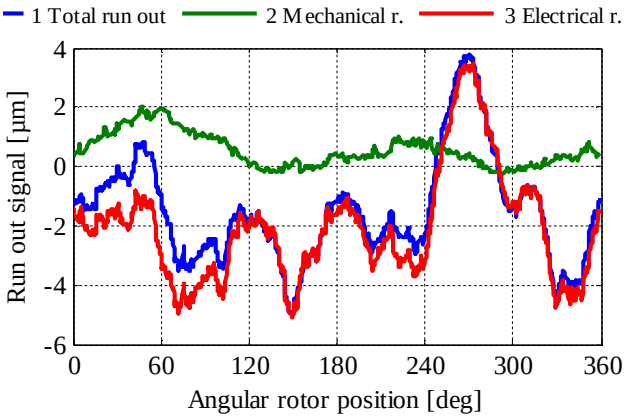

Figure 18. Run-Out Measurement for Test Sample 2.

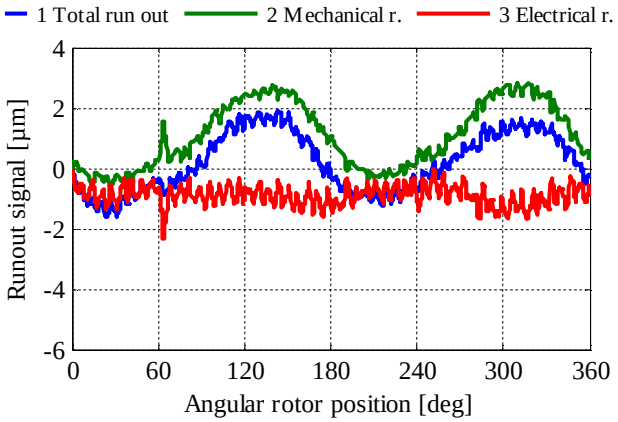

Figure 19. Run-Out Measurement for Test Sample 5.

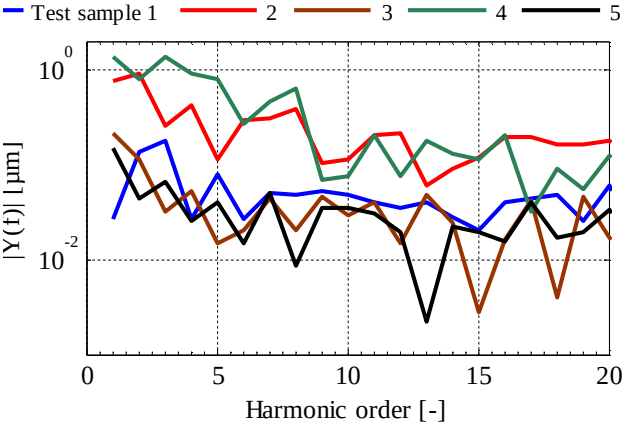

Figure 20. Fourier Transformed Electrical Run-Out Signal Portions of Five Test Samples.

calculated as the difference between the sensor signals. The mismatch of the two sensor positions as well as the material-specific measuring sensitivity of the eddy current sensor is taken into account for the data evaluation. Figure 18 and Figure 19

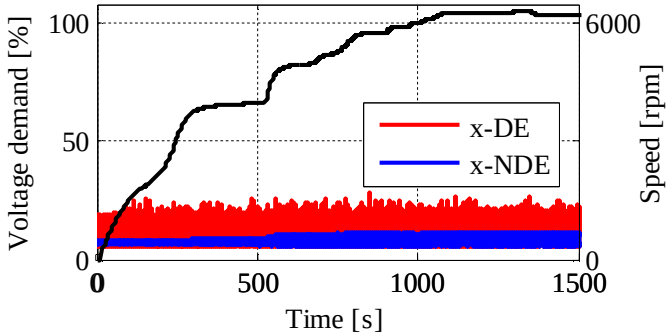

Figure 21. Voltage demand of AMB Inverters, x-DE in Comparison to x-NDE Axis for Optimized Sensor Targets

show two examples of such run-out measurements. Figure 18 shows a total run-out which is dominated by a large portion of electrical run-out. A contrary situation is shown in Figure 19: in the presence of a similar mechanical run-out, the electrical run-out portion decreased significantly by an optimized combination of material and manufacturing. The spike at 60 degrees in the mechanical and the (calculated) electrical run-out portion is caused by a marking on the shaft surface.

As a high number of super-harmonics have caused the observed 80 percent inverter voltage demand, it is not sufficient to judge the 21 test samples by their maximum peak-peak run-out values only. In order to take the effects of super-harmonics into account, the electrical portion of each run-out measurement has been Fourier transformed in order to allow for comparisons with each other test sample. Five examples of such Fourier transformed signals are presented in Figure 20.
Under consideration of the aforementioned optimization aspects, the best evaluated test sample formed the basis for the latest radial sensor target design, which already was successfully applied for a subsequent AMB supported turbo compressor, see Figure 21. For a similar combination of wide and small band radial AMB controller design the inverter voltage demand now is comparatively low for the DE: below 25 percent voltage demand in contrast to about 80 percent at 6,000 rpm before.

Optimized Axial Sensor Carrier Design

The axial sensor carrier is installed at NDE and carries four active axial sensors, which target at a sensor disc installed at the very end of the compressor shaft. The averaging of the four sensors forms the axial rotor position signal and the input of the axial AMB controller. The position of the carrier allows for easily commissioning and maintenance in case of sensor failure.

The very first design of the axial sensor carrier is shown in Figure 22, utmost to the left. In case of strong axial contacts during axial BuB tests, an axial displacement of this sensor carrier has been detected. The displacement is caused by the housing elasticity at NDE whenever the axial BuB absorbs high

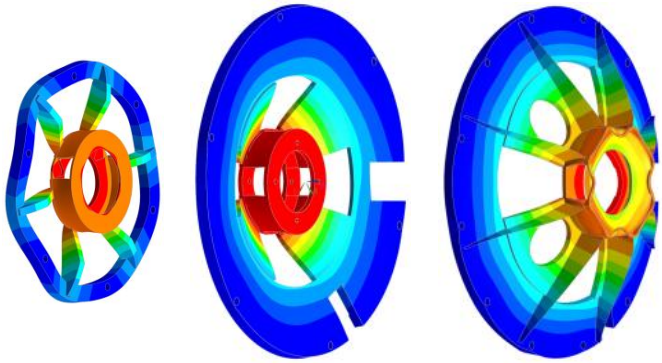

Figure 22. Axial Sensor Carrier Design Optimizations (from left to right). Illustration of the first Fundamental Mode Shape under Boundary Conditions for each of the Carrier Designs

axial loads. This causes a falsification of the axial rotor position measurement, which in turn can lead to misjudgments of the remaining service life of the axial BuB and to an oversight of possible structural damages.

To ensure reliably axial displacement measurements under all conditions, the outer radius of the axial sensor carrier is increased to allow for its installation further away from the axial BuB and closer to the stiffer compressor housing elements. But the enlarged sensor carrier in Figure 22, center positon, accompanies a lowering of the 1st fundamental resonance frequency from 635Hz to 346Hz. This reduced resonance frequency must be taken into account in the axial AMB controller design and limits the design scope of the axial controller in terms of AMB stiffness, damping and closed loop robustness. In contrast, the third and final sensor carrier design, rightmost in Figure 22, is a further redesign, which has been optimized by the internal supplier in order to combine a large installation diameter and a stiff design, providing a sufficient high fundamental resonance frequency above 600 Hz. Such a high mode can easily be controlled by gain compensation and without relevant restrictions for other AMB controller design criteria.

Torsional Train Analysis

The wide compression string speed ranging from 50 percent to 105 percent in combination with numerous noninteger harmonics of the motor inverter leads to numerous intersections with the torsional resonance frequencies of the string. Especially the intersections with the 1st and 2nd torsional resonances are

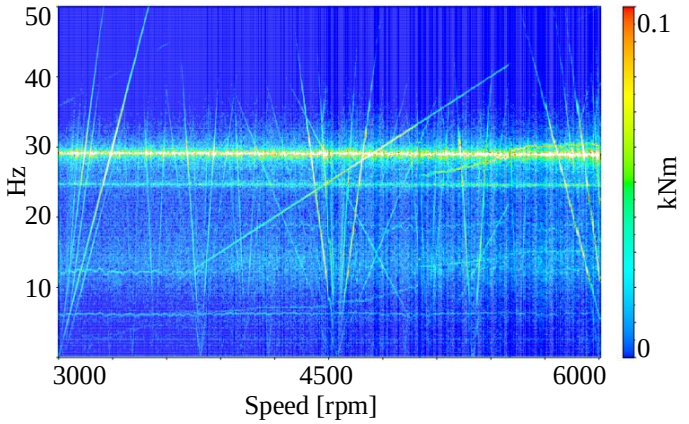

Figure 23. Campbell Diagram, Torque Measurement at 1st Section Coupling Spacer During Ramp-Up with 1 rpm / s.

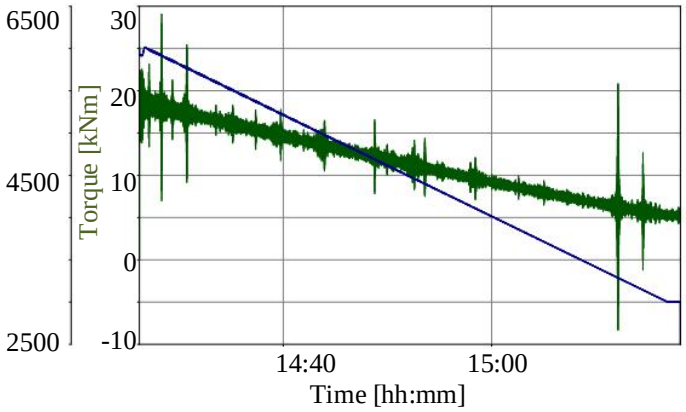

Figure 24. Torque Measurement at 1st Section Coupling Spacer During Ramp-Down from 6,000 to 3,000 rpm with -1 rpm / s

of interest due to possible significant resonance raises caused by typically low torsional damping of AMBs.

Especially the coupling selections for the 1st and 2nd section is a difficult trade-off in between fatigue and mechanical short-circuit resistance, desirable axial train dynamic, tolerable thermal expansion of the 16m long train, (overhang) coupling masses, and the degree of lateral decoupling in between the motor and the two compressors. The chosen trade-off shall also proof suitability.

Taken together, in order to validate torsional string simulations for the new compressor string design, mainly due to uncertain torsional damping and excitation of the new string, an experimental torsional analysis has been conducted by means

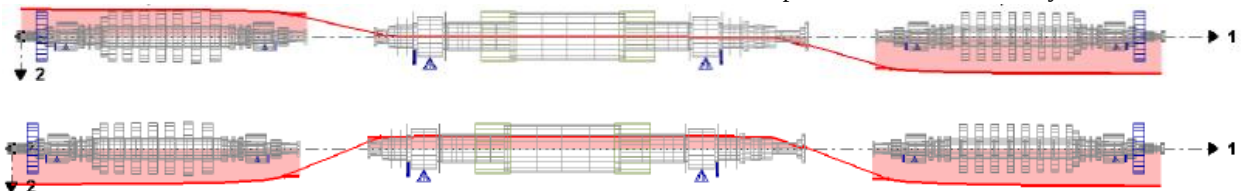

Figure 25. First Two Torsional Mode Shapes (24Hz & 28Hz)

of strain gages. The strain gages have been applied on the two coupling spacers, allowing for static and transient torque measurements. Some of the results for the somewhat stronger loaded 1st section are shown Figure 23 and Figure 24.

The Campbell Diagram in Figure 23 from 3,000rpm (50 percent) to 6,000rpm (100 percent) indicates the 1st and the 2nd torsional train resonances by two horizontal lines at about 25Hz and 29 Hz respectively. Obviously the 2nd torsional resonance at 29Hz is more pronounced due to a higher degree of excitability (confer torsional mode shapes in Figure 23). The numerous noninteger harmonic excitations caused by the motor inverter are indicated by the falling or rising lines. In the time domain, the corresponding intersection points are characterized by more or less strong resonance raises, as seen in Figure 24.

The measured resonances partially exceeded the simulated resonance peaks so that simulation data base could be updated by means of test results. Moreover, the intersection points with the second torsional resonance at about 3,290 rpm and 5,911 rpm have undergone a detailed analysis including damping determination. Despite relatively high dynamic torques at these resonance intersection points, the torsional analysis proves that the train can safely operate within its speed range and with infinite life fatigue limits.

Ready-To-Use Container Solution

The commissioning experience of the compressor train on site in Schaapbulten uncovers potential for a further reduction of the commissioning time of AMB supported compression strings by means of a ready-to-use container solution, which houses tested and precommissioned AMB cabinets. This concept has been realized for the subsequent commissioning of a 23-MW compressor.

CONCLUSION

A qualification for a large turbo compressor train with active magnetic bearings was performed according to a development release program by means of the Technology Readiness Level. After a successful component qualification in a full scale prototype compressor, the AMB System was commissioned in the pilot upstream compression train. Various robustness tests and operational experiences proved the concept with availability and reliability figures for the prototype applications of >99.9 percent in the first year of operation.

NOMENCLATURE

AMB = Active magnetic bearing
BuB = Backup Bearing
DE = Drive End
NDE = Non drive end
TRL = Technology readiness level
UPS = Uninterruptable power supply

REFERENCES

Kocur, J.A., Nicholas, J.C., Lee, C.C., 2007, Surveying Tilting Pad Journal Bearing and Gas Labyrinth Seal Coefficients and their Effect on Rotor Stability“ *Proceedings of the 36th Turbomachinery Symposium*, Turbomachinery Laboratory, Texas A&M University, College Station, TX

Kümmle, H. , Lenderink, G.M., de Groot, W.H., Shultz, R.R., 2000, Design and experience with a 30,000 HP magnetic bearing supported motor driven turbocompressor for a speed range of 600 to 6300 rpm, *Proceedings of the 29th Turbomachinery Symposium*, Texas A&M University, College Station, Texas, pp.65-80.

Swanson, E.E. , Maslen, E.H., Li, G., Cloud, C.H., 2008, Rotordynamic design audits of AMB supported machines, *Proceedings of the 37th Turbomachinery Symposium*, Texas A&M University, College Station, Texas, pp.133-158.

Walter, H., Denk, J., Stoiber, D., Köpken, H.G., 2010, Industrialization of AMB systems with standard drive technology, PCIC Europe 2010, Conference Record, pp.1-8.

Walter, H., Denk, J., Stoiber, D., 2010, Active magnetic bearing systems with standard drive technology for large turbo machines, Petroleum and Chemical Industry Conference (PCIC), Record of Conference Papers Industry Applications Society 57th Annual, pp.1-8.

ACKNOWLEDGEMENTS

The authors would like to take this opportunity to thank all those who made it possible to perform the qualification campaign. The contributions to this project from many persons, not all of whom can be listed here, are highly appreciated.